Intrinsically stealth fluorescent organic nanoparticles made of articulated bis-dipolar dyes for single particle tracking

Morgane Rosendale, Guillaume Clermont, Jonathan Daniel, Chiara Paviolo, Laurent Cognet, Jean-Baptiste Verlhac, Mireille Blanchard-Desce

Intrinsically stealth fluorescent organic nanoparticles made of articulated bis-dipolar dyes for single particle tracking

Morgane Rosendale[a], Guillaume Clermont[a], Jonathan Daniel[a], Chiara Paviolo[b], Laurent Cognet[b*], Jean-Baptiste Verlhac[a], Mireille Blanchard-Desce[a*]

[a] Institut des Sciences Moléculaires, Université de Bordeaux & CNRS, UMR 5255, 351 Cours de la Libération, 33405 Talence, France ; [b] LP2N, Université de Bordeaux, Institut d'Optique & CNRS, UMR 5298, 351 Cours de la Libération, 33405 Talence, France

ABSTRACT

Luminescent nanoparticles are becoming fundamental tools to the field of bioimaging. The optimization of their size, brightness and stability is key for applications ranging from contrast agent assisted surgery to diagnosis and therapeutics. A plethora of formulations have been documented which can be split into inorganic, organic and hybrid categories. While each class has their own advantages and limitations, controlling the interactions occurring between nanoparticles and cellular membranes is of the utmost importance. In particular, a major challenge for various applications, especially molecular imaging of membrane receptors, is to prevent non-specific interactions. Towards this goal, popular strategies based on coating nanoparticles with PEG or zwitterionic moieties have been developed to yield stealth nanoparticles. In this study, we present a series of spontaneously water-soluble and stealth organic nanoparticles. These fluorescent nanoparticles, made from original articulated bis-dipolar dyes, show vanishing interactions with living cells as bare nanoparticles. Moreover, thanks to their brightness and stability, they can be tracked as isolated single emitters in aqueous environments. These stealth nanoparticles thus hold promise for molecular imaging of specific membrane receptors, such as neuronal receptors, after bioconjugation with dedicated targeting agents.

Keywords: Luminescence, molecular-based nanoparticles, single particle tracking, stealthiness

1. INTRODUCTION

Nanotechnologies are at the heart of countless scientific advances in such various fields as computer science, energy and biomedicine. In the latter field, fluorescent nanoparticles (NPs) can be of interest as drug delivery systems[1], molecular sensors for diagnotics[2] or contrast agents for image-guided surgery[3]. They have also become ubiquitous as tools for fundamental research, such as for live cell Single Particle Tracking (SPT) and super-resolution imaging[4,5]. Despite exciting results obtained in the laboratory, the potential long-term toxicity of some nanoparticles remains to be evaluated and may be the strongest brake to clinical translation. Indeed, some of the most widely used and brightest fluorescent NPs are made of inorganic, water-insoluble and/or heavy-metal based components. These cores must thus be coated by water-soluble moieties to make them water-dispersible. Interestingly, such coatings may increase the bioavailability of inorganic NPs by acting as antifouling agents that shield them from the biological environment and prevent the accumulation of a protein corona around the circulating NP[6–8]. While successfully producing stealth NPs, the coating procedure however induces limitations of its own. These include an extra preparation step, an increase in the NP diameter and a complexification of the final product[9]. In addition, the stability of the coating in biological environments can be a critical issue, especially when the adhesion of the coating to the nanoparticle is based on non-covalent interactions.

On the road towards biocompatible nanotechnologies, Fluorescent Organic Nanoparticles (FONs) appear as an interesting alternative to inorganic NPs[10,11]. FONs are obtained *via* a bottom-up approach based on the rational design of hydrophobic dyes and their subsequent nanoprecipitation in water[12]. This rapid and green procedure allows for the fine-tuning of NP optical properties by modulating the structure of the FONs building blocks (*i.e.* dyes)[13–15].

* corresponding author: mireille.blanchard-desce@u-bordeaux.fr, laurent.cognet@u-bordeaux.fr

We recently reported on a series of FONs obtained from the nanoprecipitation of articulated bis-dipolar dyes specifically designed to promote aggregation-induced fluorescence enhancement[15]. These FONs were shown to combine exceptional brightness, absorption in the near UV-visible region, as well as a strong two-photon absorption in the near-infrared region. These organic nanoparticles also exhibit remarkable chemical and colloidal stability in pure water. Considering the interesting properties of these FONs, we hypothesized that they could be promising bioimaging tools. In this paper, we report on the usability of two of these FONs, together with FONs made of a novel dye from the same family, for single particle tracking. We found that (i) these FONs are stable for at least 24h in a cell culture system and (ii) they are intrinsically stealth, *i.e.* that they do not spontaneously interact with cellular membranes, nor get internalized by endocytosis in standard cancer cells. In addition, we demonstrate that they can be tracked as single particles in water and in protein-containing aqueous environments.

2. METHODOLOGY

2.1 FONs Preparation and characterization

200 µL of dye solution at 1 mM in THF (spectroscopic grade, Thermo Fisher) were rapidly added to 19.8 ml of freshly distilled water at room temperature under continuous sonication (10 W) for 3 min. Absorption spectra were recorded at room temperature on a Jasco V-670 UV/Vis spectrophotometer. Corrected emission spectra were obtained from diluted solutions (optical density at absorbance maximum set to ~ 0.1) excited around the absorbance maximum using a Fluorolog spectrofluorometer. 1 cm quartz cuvettes were used. Fluorescence quantum yields were determined according to standard literature procedures using fluorescein in 0.1M aqueous NaOH ($\Phi = 0.90$) as a reference. Dry NP diameters were obtained by Transmission Electron Microscopy (TEM) performed on a Hitachi H7650 electron microscope at the Bordeaux Imaging Centre core facility. Carbon-membrane coated copper grids were ionized to make them positively charged to favor electrostatic interactions with the negatively charged FONs. A drop of undiluted FONs was deposited on such grids for 1 min, dried, contrasted with a drop of uranyl-acetate for 3 min and left to dry prior to imaging. Values reported in Table 1 are median values of the size distributions determined in a semi-automated analysis using an in-house Matlab script. Hydrodynamic diameters were determined by Dynamic Light Scattering (DLS) on a Zetasizer Nano SZ-100Z Horiba instrument operating at 173°. Analyses were performed using the software supplied by the manufacturer using the "Nano" measurement mode. Values reported in Table 1 are the peak values (mode) of number based size distributions. Zeta-potential measurements and analyses were performed on the same SZ-100Z Horiba instrument.

2.2 Cell culture

HeLa cells were cultured in DMEM (Pan Biotech) supplemented with 10 % Fetal Bovine Serum (FBS) 3 times a week and maintained in an incubator at 37 °C, 5% CO_2. 48h prior to an imaging experiment, glass coverslips were cleaned by plasma (Harrick Plasma, 3 min) and sterilized in ethanol. 40.000 cells per well were then seeded on coverslips placed in a 12-well plate. 24h prior to the experiment, FONs were prepared as described above, diluted 100 times in Phosphate Buffered Saline (PBS) + 10% FBS or DMEM + 10% FBS and incubated on the cells at 37°C for 1h or overnight as indicated. On the day of the experiment, the FONs containing medium was removed and the coverslips washed with PBS + 10% FBS before being transferred to a Ludin chamber (Life Imaging Services) in which the imaging was performed.

2.3 Optical imaging

Imaging (cellular imaging and SPT) was performed on an upright epifluorescent microscope (Nikon) equipped with an Intensilight illuminator (Nikon Instruments Inc.) and an EMCCD camera (ProEM-HS, Princeton Instrument). Images and recordings were collected using a water immersion 60× objective (NA 1.0, Nikon). Incident excitation and emitted fluorescence lights were filtered using the following filters and dichroic mirrors (Semrock): excitation FF01-403/95, mirror FF458-Di02 and emission FF01-538/84 or excitation FF01-451/106, mirror FF538-Di02 and emission FF01-650/200 as indicated. Exposure times were fixed to 40 ms for fluorescence snapshots of HeLa cells and to 10 ms for videos of SPT experiments.

2.4 Single particle tracking

FONs suspensions were diluted a hundred times in mQ water or in PBS supplemented with 10% FBS. A coverslip was placed over the sample in the Ludin chamber so as to seal off a small volume of liquid. A drop of water was then added on top of the upper coverslip, allowing the objective to immerse in water without disturbing the sample. The 2D projection of 3D FON movements were recorded and then analyzed using the Fiji (ImageJ) Mosaic plugin[16] with the following parameters: Radius: 4, Cutoff: 0.001, Per/Abs: adjusted according to the signal to noise ratio of each video (typically between 0,05 and 0.25), Link Range: 3, Displacement: 3, Dynamics: Brownian. Output trajectories were exported and further analyzed with an in-house Matlab script deriving the 2D diffusion coefficient *D*. Specifically, *D* was determined as the regression coefficient of the linear fit over the first 3 points of the Mean Squared Displacement (MSD) curve of trajectories containing more than 10 datapoints[17]. The hydrodynamic diameters $Ø_{hydro}$ were then calculated from the Stokes-Einstein equation:

$$Ø_{hydro} = 2 * \frac{\kappa_B T}{6\pi\eta D} \quad (1)$$

With κ_B the Bolzmann constant, T the temperature taken as 22°C, η the viscosity of the medium taken as 1 for water and 1.01 for PBS + 10% FBS (FBS viscosity being around 1.15 mPa.s in the considered range of velocities according to [18]) and *D* the diffusion coefficient determined as described above.

3. RESULTS

3.1 Design and preparation of FONs made from articulated-dipolar dyes

In this manuscript, we extend our study of two previously reported symmetric bis-dipolar dye molecules (named **3a** and **3b** in Reference [15] and hereafter named JBV160 and JBV174 respectively) together with a third dye (JBV181) based on the same design (Figure 1). These dyes consist of two short dipolar subunits linked by a rigid fluorenyl connector. Such a molecular structure allows for conformational freedom, resulting in articulated dipoles presenting two limit conformations (Syn and Anti, see Figure 1A). The specific design of these dyes was meant to take advantage of strong dipole-dipole interactions promoted by molecular confinement, conceivably resulting in high cohesion in the aggregated state. In addition, the presence of bulky appending moieties (linear or branched alkyl chain as well as benzyl moieties) grafted on the fluorene core were meant to prevent π-π stacking which would be deleterious to fluorescence emission. From this common template, the difference between the three dyes thus lies in the nature of these side chains. They were chosen to tune the steric hindrance between individual dyes so as to influence their self-arrangement upon nanoprecipitation and consequently, possibly tune the optical properties of the resulting FONs. We had previously found that increasing the bulkiness of these side chains from *n*butyl (JBV160) to *iso*pentyl (JBV174) improved the quantum yield of the FONs. We were therefore curious to investigate the influence of bulky benzyl moieties on FONs properties. The synthesis of the resulting JBV181 dye is shown in Figure 1C.

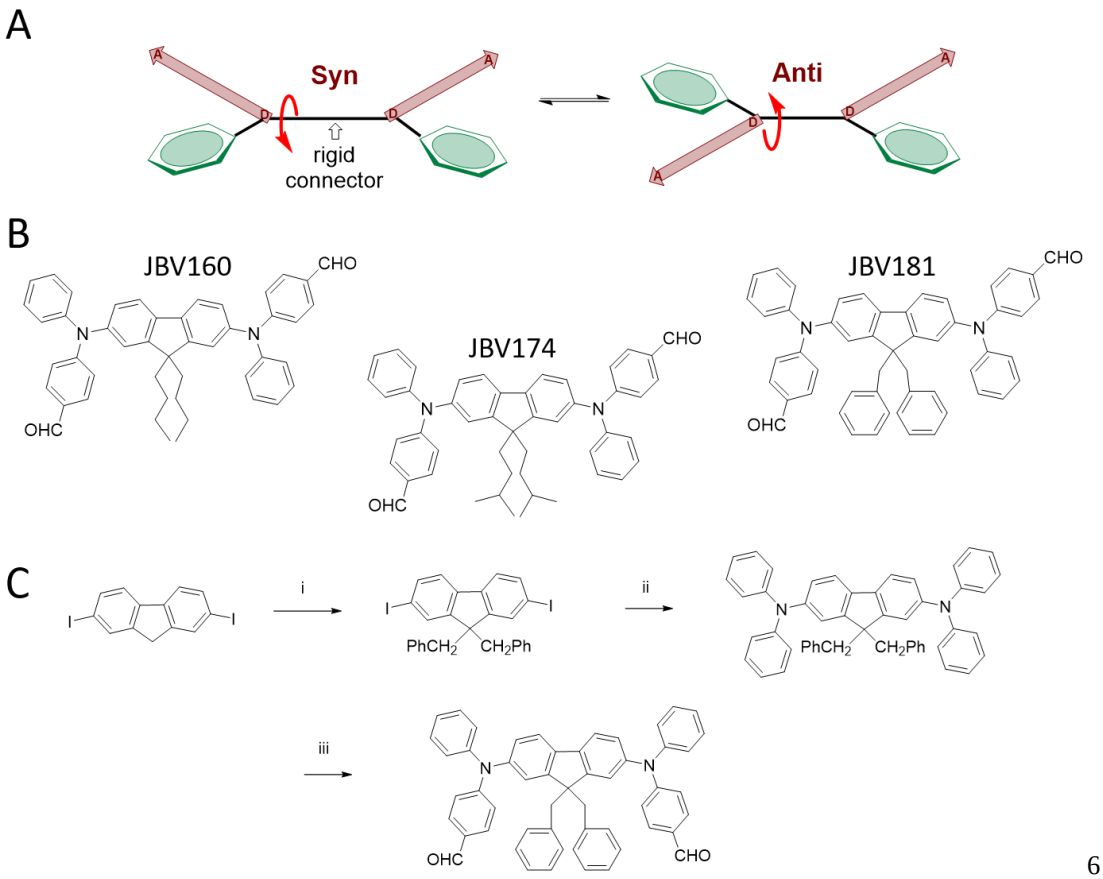

Figure 1. Articulated bis-dipolar dyes used as building blocks of the FONs characterized in this study. **A** Schematic representation of the "articulated bis-dipolar" structure. Two donor-acceptor pairs (D-A arrows) and their ballasts are arranged on each side of a rigid core around which they can rotate. **B** Chemical structures of the dyes. **C** Synthesis of dye JBV181. i: NaOH (100 eq), NaI (10% mol), $PhCH_2NEt_3Cl$ (20% mol), $PhCH_2Cl$ (6 eq) in water/toluene, 70 °C. Yield: 82% - ii: Ph_2NH, K_2CO_3, 18-Crown-6 (2% mol), Cu powder in dichlorobenzene, 200 °C. Yield: 57% - iii: $POCl_3$, DMF, 90 °C. Yield: 83%.

FONs were prepared by rapid addition of an aliquot of 1 mM solution of the articulated bis-dipolar dyes in THF into a large volume of water (1% v/v) under sonication. This simple protocol readily yielded clear transparent solutions emitting strong green fluorescence (Figure 2A). We confirmed the formation of spherical-shaped nanoparticles by Transmission Electron Microscopy (TEM) (Figure 2B) and Dynamic Light Scattering (DLS). The dry and hydrodynamic diameters obtained from TEM and DLS measurements are provided in Table 1.

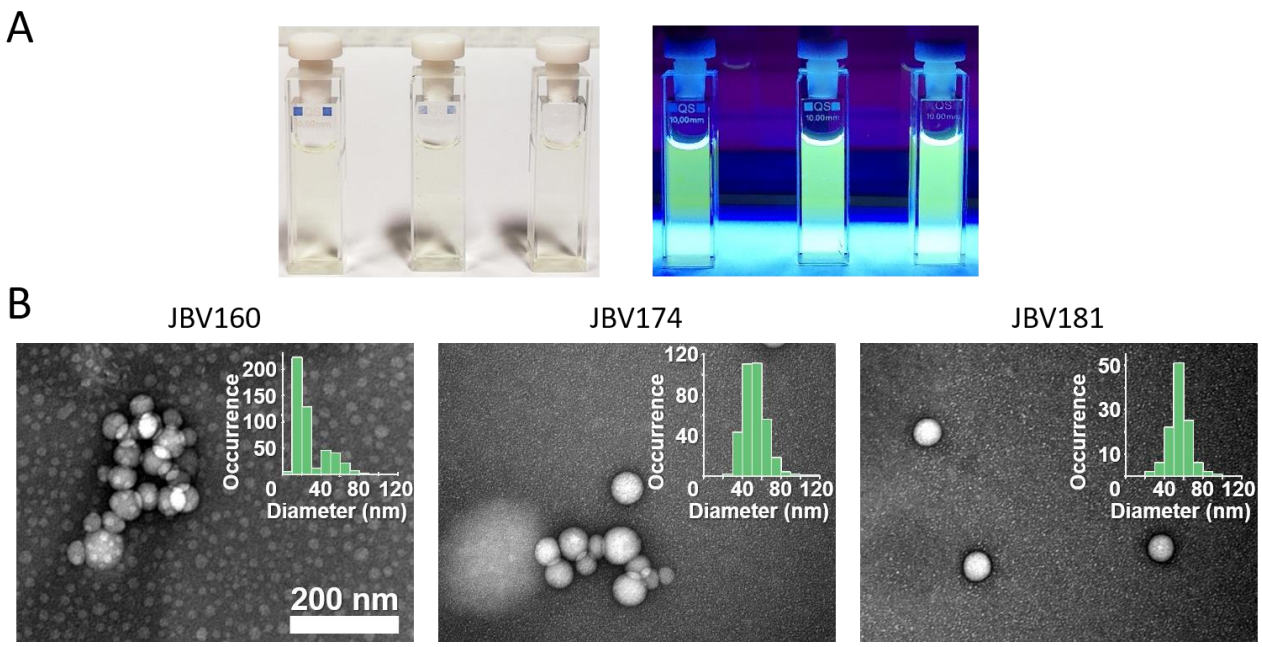

Figure 2. **A** The colloidal suspensions in water of FONs made of JBV160 (left) JBV174 (middle) and JBV181 (right) are clear and transparent (left image) and emit green fluorescence under UV light (right image); **B** Representative TEM images and size distributions (insets) of n = 488 JBV160 (left), n = 352 JBV174 (middle) and n = 116 JBV181 (right) FONs.

After nanoprecipitation in water, all dyes lead to FONs having an average dry diameter of about 55 nm – except for dye JBV160 which also yields a population of smaller nanoparticles of about 18 nm. The diameter values determined by DLS are close to those determined by TEM. The FONs also exhibit similar and markedly negative zeta potential values (Table 1). These highly negative values are anticipated to promote good colloidal properties and may hamper internalization into cells thanks to repulsive interactions with negatively charged membranes. From the size of the FONs, we can estimate the average number N of dye molecules per FON (Table 1).

Table 1. Structural characteristics of the FONs prepared by nanoprecipitation of articulated bis-dipolar dyes in water.

Dye	**$Ø_{TEM}$ [a] [nm]**	**$Ø_{hydro}^{DLS}$ [b] [nm]**	**ζ [c] [mV]**	**N [d]**
JBV160	18 / 56 *	60	-71	3000 / 83000
JBV174	53	50	-67	67000
JBV181	56	60	-64	75000

[a] Dry diameter of the FONs measured by TEM. * Two populations were observed in JBV160 TEM images. The mean diameter of the overall population is 29 nm; [b] Hydrodynamic diameter derived from DLS experiments; [c] Zeta potential; [d] Average number of dye molecules per FON calculated from the dry diameter ($Ø_{TEM}$) assuming a density of 1.

3.2 Optical properties of the dyes and FONs

We next investigated the optical properties of the FONs. Firstly, we compared the photophysical properties of the dyes as isolated molecules in THF and as aggregated subunits of FONs in water. The obtained data are provided in Table 2.

Table 2. Comparison of the photophysical properties of bis-dipolar dyes in THF and as subunits of FONs in water

Dye	λ_{abs}^{max} a) [nm]	ε^{max} b) [$10^4.M^{-1}.cm^{-1}$]	λ_{em}^{max} c) [nm]	Φ_f d)	τ e) [ns]
JBV160 dye/THF [15]	382	5.6	530	0.11	2.2
FONs/H_2O	380	4.7	513	0.13	1.5 (46%) 4.8 (54%)
JBV174 dye/THF [15]	381	5.3	530	0.10	1.8
FONs/H_2O	381	4.6	511	0.16	1.6 (41%) 5.0 (59%)
JBV181 dye/ THF	374	5.1	525	0.12	2.0
FONs/H_2O	374	4.2	510	0.18	1.9 (40%) 5.7 (60%)

a) Absorbance maximum wavelength; b) Molar attenuation coefficient of the dye at λ_{abs}^{max}; c) Emission maximum wavelength; d) Fluorescence quantum yield; e) Fluorescence lifetime. When decay is multi-exponential, the contribution of each lifetime value to the fit is indicated between brackets.

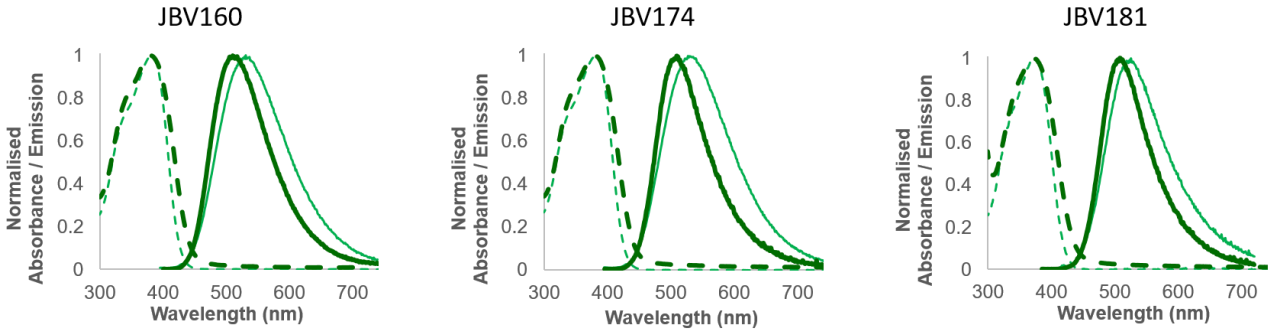

Figure 3. Normalized absorbance (dashed lines) and emission (solid lines) spectra of the dyes in THF (thin, light green lines) and in FONs (thick, dark green lines).

We observe that the dyes show similar absorption spectra in both THF and water, except for a slight broadening of the absorption band upon aggregation (Figure 3). We also note that the molecular confinement induces a decrease of their molar absorption coefficient. This decrease ranges from 13% for JBV174 to 16% for JBV160 and to 18% for JBV181 (Table 2). Comparison of the fluorescence emission spectra evidences a slight hypsochromic shift for aggregated dyes (Figure 3). Interestingly, an increase in the fluorescence quantum yield values is also observed (Table 2). This behavior is reminiscent of the so-called aggregation induced emission enhancement. The emission enhancement appears to follow the steric hindrance of the side chains located on the fluorene core. The bulkier *iso*pentyl chains (JBV174) leads to the largest enhancement (60 %), close to that generated by the benzyl side chains of JBV181 (50 %), compared to that observed for the *n*butyl side chains of JVB160 (27%). These data support our rational that the presence of bulky side chains on the fluorene core are beneficial to the fluorescence properties of the nanoparticles, most probably by hindering interchromophoric interactions that are deleterious to fluorescence emission.

Table 3. Optical properties of the FONs made from articulated bis-dipolar dyes.

Dye	λ_{abs}^{max} a) [nm]	ε_{FONs}^{max} b) [$10^9.M^{-1}.cm^{-1}$]	λ_{em}^{max} c) [nm]	Φ_f d)	$\varepsilon.\Phi_f$ e) [$10^8.M^{-1}.cm^{-1}$]
JBV160	380	0.12 / 3.7	513	0.13	0.16 / 4.8
JBV174	381	3.3	511	0.16	5.7
JBV181	374	3.2	510	0.18	5.6

a) Absorbance maximum wavelength; b) Molar attenuation coefficient of the FONs at λ_{abs}^{max}; c) Emission maximum wavelength; d) Fluorescence quantum yield; e) Brightness.

Thanks to the confinement of a large number of dyes per FON, the FONs show huge molar absorption coefficients, resulting in giant brightness (Table 3). In addition, as expected from the very negative zeta potential values, we confirmed that all obtained FONs show good colloid stability. Indeed, we observed no visible aggregation in the samples and the absorbance spectra remained virtually unchanged over the course of two weeks (Figure 4).

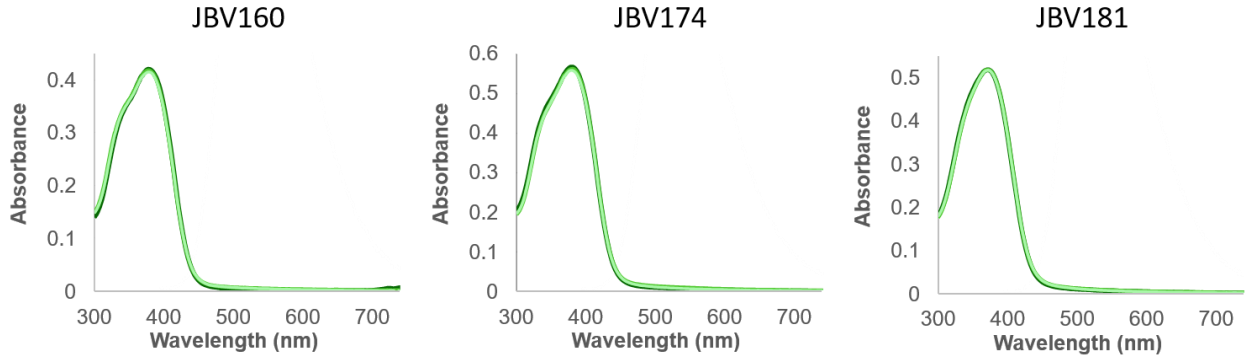

Figure 4. Superimposed absorbance spectra of the FONs colloidal suspensions measured on the day of FONs preparation (dark green), 7 days later (green) and 14 days later (light green).

Having confirmed the attractive optical properties and the stability of these molecular-based nanoparticles in water, we wanted to assess their usability for optical microscopy and bioimaging.

3.3 Single particle tracking of FONs in pure water and in a model physiological medium

We used single particle tracking (SPT) as a means of monitoring the integrity and brightness of FONs in a model physiological medium. Indeed, SPT is a powerful microscopy technique, often used in combination with fluorescent nanoparticles to study the dynamics of biomolecules and the intrinsic properties of bioenvironments. As a proof of principle, we first observed the FONs' Brownian motion in water by SPT. When excited around their maximum absorbance (excitation filter centred on 403 nm, emission collected around 650 nm), FONs were bright enough to be imaged with exposure times as short as 10 ms, an important parameter for successful tracking of diffusing nano-objects. Indeed, as smaller objects move faster, shorter acquisition times allow for a robust reconnection of particle centroids into trajectories using the ImageJ Mosaic plugin (Figure 5A). Of note, photobleaching was visible over the field of view within a few tens of seconds, FONs made from dye JBV181 being the most photostable among the series. However, and despite signals expectedly getting lost as NPs moved along the z-axis, individual FONs were bright and stable enough to be tracked for tens to hundreds of datapoints while in the depth-of-focus of the microscope. In other words, trajectories were long enough to calculate the 2D diffusion coefficient of individual FONs and infer their hydrodynamic diameter using the Stokes-Einstein equation (See section 2.4). The obtained diameters, around 55 nm for all FONs (Table 4, Figure 5E), are in good agreement with values obtained from TEM and DLS measurements (Table 1).

Table 4. Hydrodynamic diameters of FONs obtained by Single Particle Tracking

Dye	$Ø_{hydro}$ SPT in H2O a) [nm]	$Ø_{hydro}$ SPT in PBS+FBS b) [nm]
JBV160	53	85
JBV174	55	81
JBV181	62	84

[a)] Hydrodynamic diameter derived from tracking the Brownian motion of n = 141 for JBV160, n = 275 for JBV174 and n = 521 for JBV181 FONs in water; [b)] Hydrodynamic diameter derived from tracking the Brownian motion of n = 37 for JBV160, n = 70 for JBV174 and n = 88 for JBV181 FONs in PBS + 10% FBS

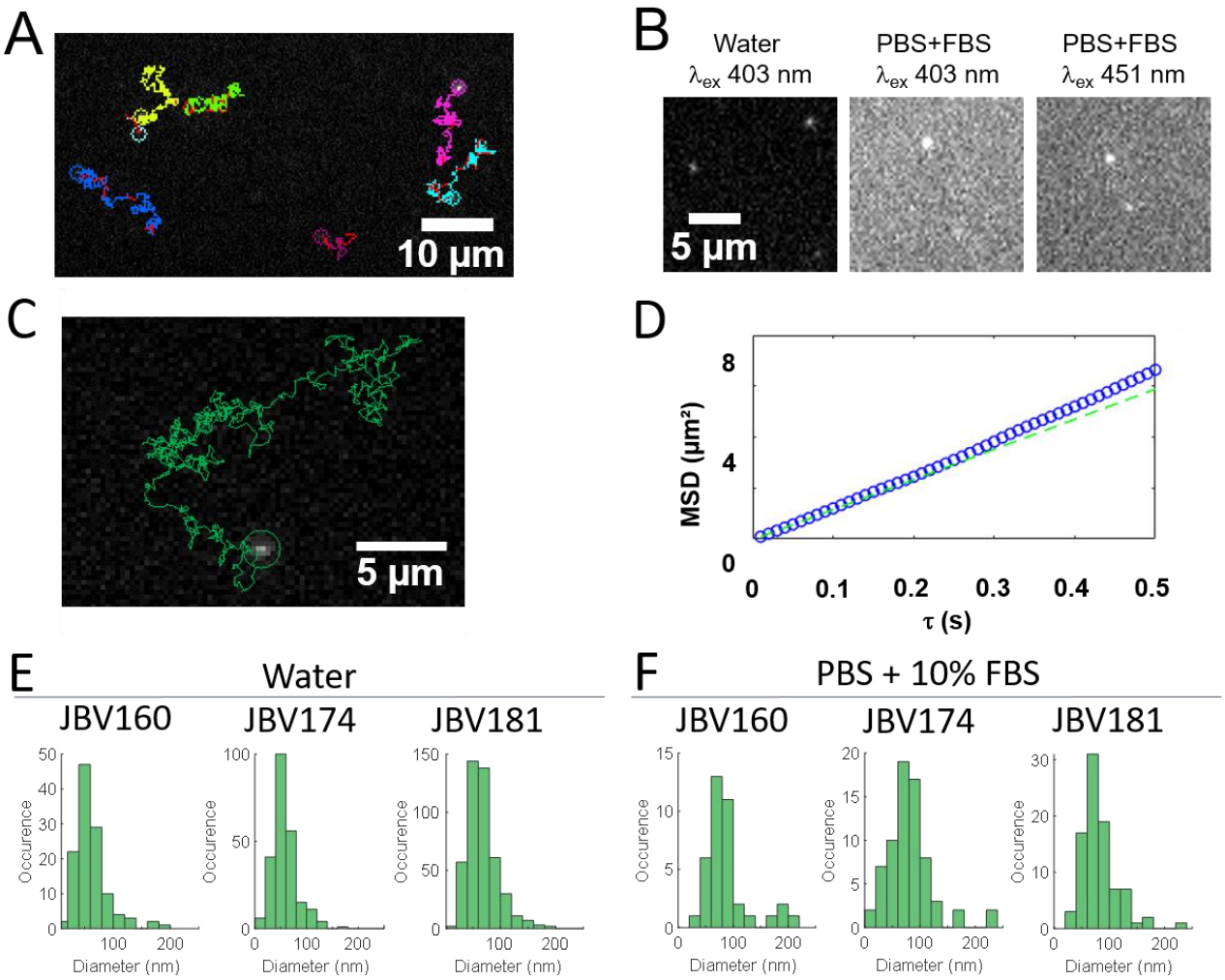

Figure 5. **A** JBV160 FONs in water tracked using Mosaic software. Individual tracks recognized as a belonging to the same trajectory are colour-coded. Red lines indicate reconnections when the track was lost for 1 to 3 frames. **B** JBV174 FONs imaged in the indicated medium and excited at the indicated wavelength. All three images are displayed using the same grayscale for comparison. **C** Example JBV181 FON tracked for more than 10 s in PBS + 10% FBS. **D** MSD curve corresponding to the trajectory shown in C. The linear fit calculated over the first 3 points of the MSD and used to determine the diffusion coefficient is displayed as a green dashed line. **E-F** Histograms of size distributions of FONs in water (E) and in PBS + 10% FBS (F).

We then tracked the motion of FONs in Phosphate Buffered Saline supplemented with Foetal Bovine Serum (PBS + 10% FBS) as a model physiological environment. Our first observation was that punctate, rapidly moving emitters could be seen, indicating that FONs do not fully disintegrate nor dramatically aggregate in a saline, protein containing environment. However, the signal to noise ratio dramatically decreased in the presence of FBS (Figure 5B). We could analyse roughly 30 trajectories per condition under those conditions, yielding hydrodynamic diameters of 83, 80 and 81 nm for JBV160, JBV174 and JBV181 FONs respectively. However, violet light being suboptimal for optical microscopy, we tested whether FONs could be better detected using a slightly more red-shifted excitation light (centred around 451 nm, see Section 2.4). Despite exciting further away from the absorbance maximum of the FONs, the signal improved sufficiently to allow the tracking of almost twice as many trajectories (Figure 5B-D). The hydrodynamic diameters obtained from those measurements are provided in Table 4 (also see Figure 5F). We observe that the apparent hydrodynamic diameters of FONs increase by ~25 nm in the presence of PBS and FBS as compared to water. This indicates that FONs largely maintain their integrity under those conditions. Indeed, if most FONs aggregated due to the change in medium, the increase in the hydrodynamic diameters of the resulting FON clusters should be larger than what is observed. Therefore, these results most likely suggest the formation of a protein corona around individual nanoparticles.

As such coronas are known to influence the interaction between NPs and cellular membranes, we moved on to investigate the behaviour of FONs in a cellular environment.

3.4 Stealth behavior of FONs towards live HeLa cells

We first investigated the behavior of FONs towards HeLa cells, a model cancer cell line. We assessed their biocompatibility by incubating the FONs for 24h on the cells. To do so, we directly added the nanoparticles (1% v/v) to the cell culture medium consisting of DMEM supplemented with FBS. We noticed no signs of cytotoxicity after such incubation. Most interestingly, while previously reported NIR-emitting FONs built from dipolar dyes tended to internalize into COS-7 cells[19], we found that after 24h incubation, none of the three FONs tested here were observed to stick to cell surfaces, nor to accumulate intracellularly (Figure 6).

These preliminary experiments suggest that these FONs behave as spontaneously stealth nanoparticles, requiring no specific coating to prevent interactions with cellular membranes. Further studies will be required to assess if this behavior is universal to different cell types.

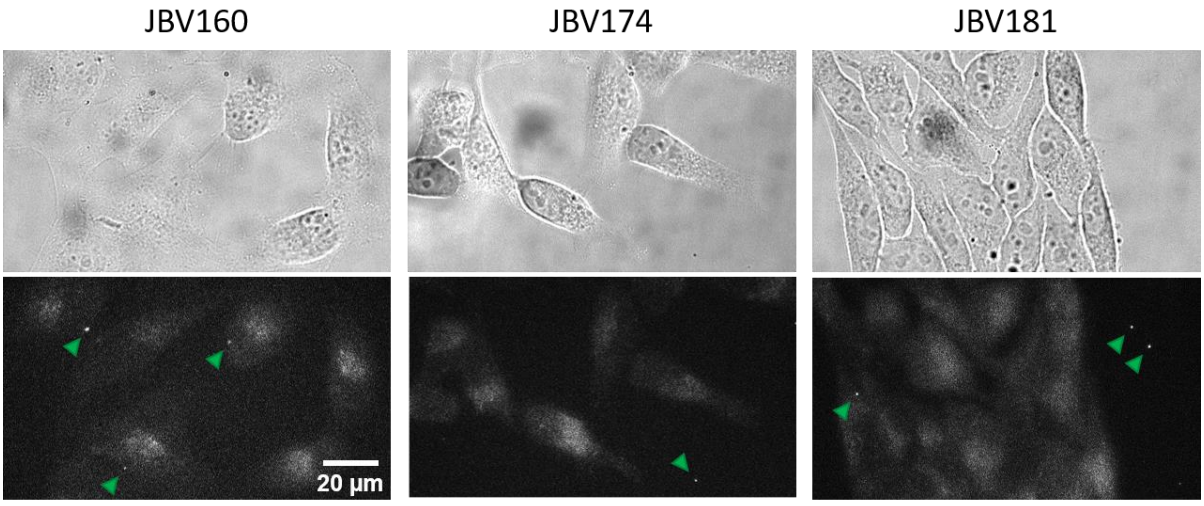

Figure 6. FONs have no unspecific interactions with biological membranes. Left: JBV160, Middle: JBV174, Right: JBV181. Upper panel: Bright field images of HeLa cells incubated for 24h with FONs exhibiting no apparent cell death. Lower panel: Fluorescence images of the same field of view as in the upper panel. Excitation light centred around 403 nm, Emission light collected around 538 nm (See Section 2.4). FONs fluorescence can be observed in punctate emitters (arrowheads) but these are seldom found. When so, FONs have been observed on both the cells and the coverslips, suggesting neither uptake nor preferential accumulation inside the cells.

4. CONCLUSION

In this study, we investigated the potential of a series of molecular-based fluorescent nanoparticles made of bis-dipolar dyes for single particle tracking in biological environment. This molecular design was previously demonstrated to yield nanoparticles that show large brightness (in relation with aggregation induced emission enhancement) and good colloidal stability in pure water. We have shown that the FONs derived from this series can be used in optical microscopy applications.

Previous work from our laboratory had shown that different dye designs strongly influence the stability of FONs in physiological environments[20]. While the two dyes presented in this early study were derived from a shared triphenylamine motif, FONs made of a dipolar dye could be imaged more than an hour after injection in blood vessels whereas FONs made of an octupolar dye aggregated within minutes, leading to the death of the experimental organism. Here, we show that the FONs derived from the new, also triphenylamine-based, bis-dipolar design induce no apparent cytotoxicity after 24h incubation with HeLa cells. Importantly, they also do not accumulate intracellularly. These FONs thus behave as spontaneously stealth nanoparticles towards this type of cells. It will be interesting to investigate if this characteristic holds true in other cell types and if the FONs display reduced clearance when injected in the bloodstream. If they remain spontaneously stealth in complex environments such as in tissues or *in vivo*, these all organic, small (<100 nm) and bright NPs may find their way to many bioimaging applications as a new class of nanoprobes.

Also, we showed that these FONs combine sufficient brightness and photostability to be detected as single emitters and used in single particle tracking experiments. As a proof of principle, we measured the hydrodynamic diameters of these FONs in water and in a model physiological medium (PBS + 10% FBS). These measurements revealed a ~25 nm increase in the apparent hydrodynamic diameters in the presence of FBS. This suggests that serum proteins do interact - most probably via electrostatic interactions - with the surface of the nanoparticles, resulting in the formation of a thick protein corona. This observation raises the question of the potential role of this protein corona on the paucity of interactions between these FONs and cellular membranes and the stealth behavior of these FONs. Interesting neuroscience applications for which stealth nanoparticles will be promising, and for which single particle tracking is a method of choice to access diffusion parameters, are the study of the brain extracellular space[21] and of the dynamics of neurotransmitter membrane receptors[22].

Many potential future developments can be envisaged for the FONs presented in this study. Among others, it should be interesting to try and biofunctionalize them with targeting moieties. These could include ligands displaying a pharmaceutical action on target cells or recognition elements such as antibodies, for example to perform single particle tracking of cell surface receptors. Another interesting perspective for *in vivo* imaging would be to tune the emission of such dyes to more red-shifted wavelengths o as to match the transparency window of biological tissues. Taken together, these FONs should prove a new and versatile tool in the bioimaging toolbox.

ACKNOWLEDGMENTS

This work has received funding from the European Union's Horizon 2020 research and innovation program under the Marie Skłodowska-Curie grant agreements n° 841379 to M.R. and n°793296 to C.P. The work was performed in the frame of the "DynHippo" project (ANR-15-CE16-0004) and was supported by the LAPHIA Cluster of Excellence. Transmission electron microscopy was done in the Bordeaux Imaging Center, a service unit of the CNRS-INSERM and Bordeaux University, member of the national infrastructure France Bioimaging supported by the French National Research Agency (ANR-10-INBS-04).

REFERENCES

[1] Duncan, B., Kim, C. and Rotello, V. M., "Gold nanoparticle platforms as drug and biomacromolecule delivery systems," Journal of Controlled Release **148**(1), 122–127 (2010).

[2] Xiong, J., Cao, X., Yang, S., Mo, Z., Wang, W. and Zeng, W., "Fluorescent Probes for Detection of Protein: From Bench to Bed," Protein Pept. Lett. **25**(6), 548–559 (2018).

[3] Tanaka, E., Choi, H. S., Fujii, H., Bawendi, M. G. and Frangioni, J. V., "Image-Guided Oncologic Surgery Using Invisible Light: Completed Pre-Clinical Development for Sentinel Lymph Node Mapping," Ann Surg Oncol **13**(12), 1671–1681 (2006).

[4] Cognet, L., Leduc, C. and Lounis, B., "Advances in live-cell single-particle tracking and dynamic super-resolution imaging," Current Opinion in Chemical Biology **20**, 78–85 (2014).

[5] Bannai, H., "Molecular membrane dynamics: Insights into synaptic function and neuropathological disease," Neurosci. Res. **129**, 47–56 (2018).

[6] Karakoti, A. S., Das, S., Thevuthasan, S. and Seal, S., "PEGylated Inorganic Nanoparticles," Angewandte Chemie International Edition **50**(9), 1980–1994 (2011).

[7] García, K. P., Zarschler, K., Barbaro, L., Barreto, J. A., O'Malley, W., Spiccia, L., Stephan, H. and Graham, B., "Zwitterionic-Coated 'Stealth' Nanoparticles for Biomedical Applications: Recent Advances in Countering Biomolecular Corona Formation and Uptake by the Mononuclear Phagocyte System," Small **10**(13), 2516–2529 (2014).

[8] Ahsan, S. M., Rao, C. M. and Ahmad, Md. F., "Nanoparticle-Protein Interaction: The Significance and Role of Protein Corona," [Cellular and Molecular Toxicology of Nanoparticles], Q. Saquib, M. Faisal, A. A. Al-Khedhairy, and A. A. Alatar, Eds., Springer International Publishing, Cham, 175–198 (2018).

[9] Shreffler, J. W., Pullan, J. E., Dailey, K. M., Mallik, S. and Brooks, A. E., "Overcoming Hurdles in Nanoparticle Clinical Translation: The Influence of Experimental Design and Surface Modification," International Journal of Molecular Sciences **20**(23), 6056 (2019).

[10] Fery-Forgues, S., "Fluorescent organic nanocrystals and non-doped nanoparticles for biological applications," Nanoscale **5**(18), 8428 (2013).

[11] Masuhara, H., Nakanishi, H. and Sasaki, K., eds., [Single Organic Nanoparticles], Springer Berlin Heidelberg, Berlin, Heidelberg (2003).

[12] Horn, D. and Rieger, J., "Organic Nanoparticles in the Aqueous Phase-Theory, Experiment, and Use," Angew. Chem. Int. Ed. Engl. **40**(23), 4330–4361 (2001).

[13] Ishow, E., Brosseau, A., Clavier, G., Nakatani, K., Tauc, P., Fiorini-Debuisschert, C., Neveu, S., Sandre, O. and Léaustic, A., "Multicolor Emission of Small Molecule-Based Amorphous Thin Films and Nanoparticles with a Single Excitation Wavelength," Chem. Mater. **20**(21), 6597–6599 (2008).

[14] Mastrodonato, C., Pagano, P., Daniel, J., Vaultier, M. and Blanchard-Desce, M., "Molecular-Based Fluorescent Nanoparticles Built from Dedicated Dipolar Thienothiophene Dyes as Ultra-Bright Green to NIR Nanoemitters," Molecules **21**(9) (2016).

[15] Verlhac, J.-B., Daniel, J., Pagano, P., Clermont, G. and Blanchard-Desce, M., "Enhanced two-photon brightness in molecular-based organic nanoparticles built from articulated-dipoles," Comptes Rendus Chimie **19**(1–2), 28–38 (2016).

[16] Sbalzarini, I. F. and Koumoutsakos, P., "Feature point tracking and trajectory analysis for video imaging in cell biology," J. Struct. Biol. **151**(2), 182–195 (2005).

[17] Kusumi, A., Sako, Y. and Yamamoto, M., "Confined lateral diffusion of membrane receptors as studied by single particle tracking (nanovid microscopy). Effects of calcium-induced differentiation in cultured epithelial cells," Biophysical Journal **65**(5), 2021–2040 (1993).

[18] Zhang, Y., Wu, X., Wang, Y., Zhu, S., Gao, B. Z. and Yuan, X.-C., "Measurement of the microscopic viscosities of microfluids with a dynamic optical tweezers system," Laser Phys **24**(6), 065601 (2014).

[19] Genin, E., Gao, Z., Varela, J. A., Daniel, J., Bsaibess, T., Gosse, I., Groc, L., Cognet, L. and Blanchard-Desce, M., "'Hyper-bright' near-infrared emitting fluorescent organic nanoparticles for single particle tracking," Adv. Mater. Weinheim **26**(14), 2258–2261, 2257 (2014).

[20] Parthasarathy, V., Fery-Forgues, S., Campioli, E., Recher, G., Terenziani, F. and Blanchard-Desce, M., "Dipolar versus octupolar triphenylamine-based fluorescent organic nanoparticles as brilliant one- and two-photon emitters for (bio)imaging," Small **7**(22), 3219–3229 (2011).

[21] Godin, A. G., Varela, J. A., Gao, Z., Danné, N., Dupuis, J. P., Lounis, B., Groc, L. and Cognet, L., "Single-nanotube tracking reveals the nanoscale organization of the extracellular space in the live brain," Nat Nanotechnol **12**(3), 238–243 (2017).

[22] Varela, J. A., Dupuis, J. P., Etchepare, L., Espana, A., Cognet, L. and Groc, L., "Targeting neurotransmitter receptors with nanoparticles in vivo allows single-molecule tracking in acute brain slices," Nat Commun **7**, 10947 (2016).